Int. J. Electrochem. Sci., 7 **(2012)** 7111 - 7120

International Journal of
ELECTROCHEMICAL
SCIENCE
www.electrochemsci.org

The Comparison of Carbon Conductive Additives with Different Dimensions on the Electrochemical Performance of $LiFePO_4$ Cathode

X.L. Li[*], *Y.L. Zhang, H.F. Song, K. Du, H. Wang, H.Y. Li, J.M. Huang*

School of Materials Science and Engineering, Chongqing University, Chongqing, 400030, P. R. China
[*]E-mail: lixinlu@cqu.edu.cn

Received: 26 June 2012 / *Accepted:* 18 July 2012 / *Published:* 1 August 2012

Carbon black, multi-walled carbon nanotubes and graphene nanosheets were respectively added to $LiFePO_4$ particles as conductive additives to investigate the influence on the electrochemical performance. The specific surface area and pore size distribution of $LiFePO_4$ particles were measured by N_2 absorption. The microstructure of carbon conductors and $LiFePO_4$ sample were characterized by X-ray diffraction, scanning electron microscopy and high-resolution transmission electron microscopy, respectively. The results of electrochemical measurements indicated that $LiFePO_4$ mixed with graphene nanosheets exhibited the best electrochemical performance, of which the specific capacity was up to 146 mAh g^{-1} at 0.1 C and 125 mAh g^{-1} at 1 C. Graphene nanosheets showed plane-to-point electric contact with $LiFePO_4$ particles, owing to the unique two-dimensional planar structure. In this work, it was demonstrated that graphene nanosheets will be the most promising carbon conductive additives in cathode materials for lithium-ion batteries.

Keywords: Carbon Conductive additives, graphene nanosheets, $LiFePO_4$, lithium-ion batteries

1. INTRODUCTION

Currently, the rapid development of portable energy-storage devices, especially lithium-ion rechargeable batteries, draws extensive attention due to their high operative potential and energy density as well as large capacity [1]. Since the first report from Padhi et al [2], $LiFePO_4$ has intrigued significant passion of researchers because of its cost-effectiveness, environmental benignity, excellent thermal stability and electrochemical stability [3-7]. However, both the poor intrinsic electronic and ionic conductivity seriously hamper its widespread application in high power lithium-ion batteries for commercial electric vehicles (EV) and portable electronics [8].

Enormous approaches have been taken to overcome drawbacks of $LiFePO_4$, such as carbon coating on the surface [9] or fabrication within carbonaceous matrix [4, 10-12], doping with guest metallic cations [13] and minimizing the particles size [14]. Notably, conductive additives play an important role in electrochemical performance of lithium-ion batteries. Carbonaceous materials with different dimensions, carbon black (CB) and multi-walled carbon nanotubes (CNTs), for instance, are widely used as conductive additives in electrodes for lithium-ion batteries. Park et al [15] explored the proportion of CB and CNTs in $LiCoO_2$. They found that the cathode mixed with 8 wt% CNTs exhibit the high discharge capacity of 136 mAh g^{-1} at 5 C rate. Li et al [10] prepared a novel three-dimensional network $LiFePO_4$ mixed with 5 wt% CNTs and achieved the discharge capacity of 122 mAh g^{-1} at 5 C rate. However, graphene nanosheets (GNs) have been rarely focused on as conductive additives in previous reports. Moreover, the network structure of $LiFePO_4$ mixed with different carbon conductive additives has not been systematically investigated.

Herein, CB, CNTs and GNs were respectively added to $LiFePO_4$ to construct different conducting networks, and the influence of carbonaceous conductive additives in different dimensions on the electrochemical performance of $LiFePO_4$ cathode was investigated. And the mechanism of enhancement in conductivity was further discussed.

2. EXPERIMENTAL

2.1. Materials Preparation and Cells Assembly

All chemicals were used as received without further purification. CNTs (>95%, D_{50}=20~30 nm, prepared by chemical vapor deposition with slight hydroxyls) were purchased from Timesnano, (Chengdu Organic Chemicals Co. Ltd., Chinese Academy of Sciences). The CB particles, Celgard 2500 membranes (thickness of 25 μm), $LiFePO_4$ (D_{50}=4.75 μm) sample and polyvinylidene fluoride (PVDF, used as binder) were provided by JingRui Battery Co. Ltd. (Guangzhou, China). GNs were prepared by a modified Hummers method [16]. Typically, graphite flakes were suffered from strong oxidation to get graphite oxide (GO). The resulted colloidal suspension of graphite oxide (GO) was dried at 60 ℃ under air for 48 h to get GO. Then the GO was expanded in a microwave oven (MIDEA, 800W) for 1 min. Finally, the resulted fluffy powder was dispersed in ethanol and vibrated under 150 W ultrasonication for 2 hours to produce GNs.

For cells assembly, the mixture of $LiFePO_4$ sample, carbon conductive additives and binder was dispersed in N-methyl-2-pyrrolidone (NMP, >99.9%, Alfa Aesar) in the weight ratio of 90:5:5 to make slurry. Then it was smeared uniformly on an aluminium foil current collector and dried at 80 ℃ overnight in a vacuum furnace. Afterwards, the CR2430 coin-type cells were assembled in an argon-filled glove box, while the $LiFePO_4$-based electrode as cathode, $LiPF_6$ (1.0 M in a 1:1 v/v ethyl carbonate/ diethyl carbonate mixture) as the electrolyte, Celgard 2500 membrane as a separator, lithium foil as the counter electrode and reference electrode. For comparison, the electrodes of $LiFePO_4$ added with CB, CNTs and GNs were denoted as LFP-CB, LFP-CNTs, LFP-GNs, respectively.

2.2. Sample Characterization and Electrochemical Measurements

The crystal structure was examined by X-ray diffraction (XRD) and the XRD patterns were recorded by DMAX-2500PC with Cu Kα radiation (λ=1.5406 Å). The 2-theta angle was from 15° to 70° for $LiFePO_4$ sample and 10° to 60° for carbonaceous conductive additives at the scanning speed of 4° min^{-1} respectively. Specific surface area (SSA) and pore size distribution were measured by nitrogen absorption using automatic SSA measuring equipment (ASAP 2020 M). The morphology and microstructure of specimens were observed by scanning electron microscope (SEM, FEI Nova 400) and high-resolution transmission electron microscope (HRTEM, LIBRA 200FE).

The electrochemical tests were performed at room temperature. Electrochemical impedance spectroscopy (EIS) and cyclic voltammetry (CV) were measured on an electrochemical workstation (Solartron 1287+1260 8w). CV was carried out at the scanning rate of 0.05 mV/s between 2.5 and 4.4 V, 2.3 and 4.2 V, 2.7 and 4.2 V (vs. Li/Li^+) for LFP-CB, LFP-CNTs, LFP-GNs, respectively. EIS measurements were performed over a frequency range from 100 kHz to 0.1 Hz. The galvanostatically charge-discharged performance was tested between 2.7 to 4.2 V (vs. Li/Li^+) at different rates with NBBAITE Battery Test System (NBT Co. Ltd., China).

3. RESULTS AND DISCUSSION

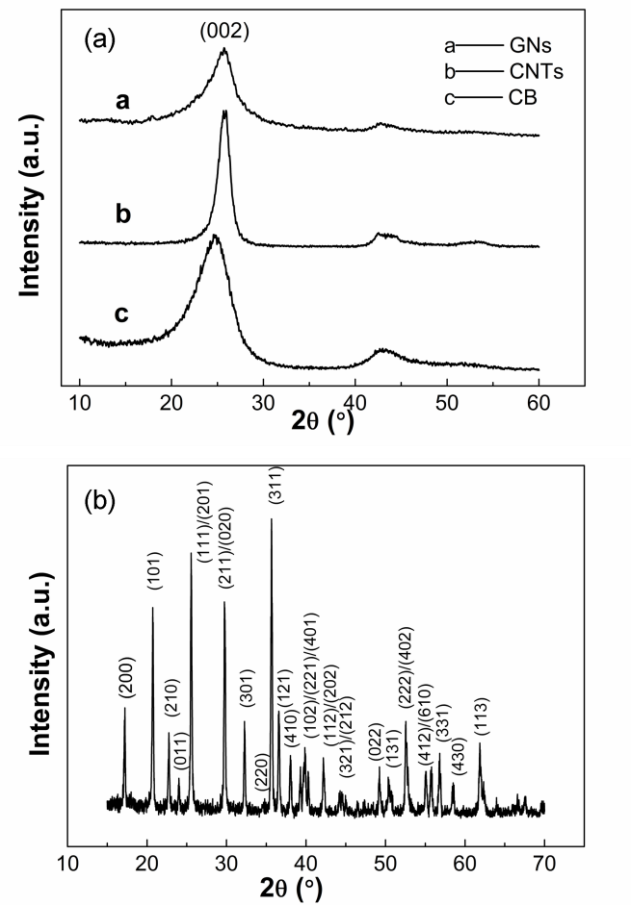

Figure 1. XRD patterns of (a) carbon conductive additives and (b) $LiFePO_4$ particles.

Fig. 1 shows the XRD patterns of the carbonaceous conductive additives (a) and $LiFePO_4$ sample (b). For the peak of (002) plane, GNs and CB exhibited relatively broad peak and low intensity in Fig.1 (a), which can be attributed to the lower graphitization resulted from defects and partial disorderness. The larger interlayer spacing of GNs (0.356 nm) was induced by intercalation and rapid expansion. The XRD of $LiFePO_4$ sample in Fig.1 (b) proves its olivine-type structure indexed to the orthorhombic *Pnma* space group (JCPDS NO. 83-2092). No peaks of impurity were found. A least squares method using six diffraction lines was conducted to calculate its cell parameters, *a*, *b* and *c*, resulting that *a* was 0.608 nm, *b* was 1.033 nm, *c* was 0.469 nm, respectively. The high intensity of the sharp diffraction peaks suggests the high crystallinity of $LiFePO_4$.

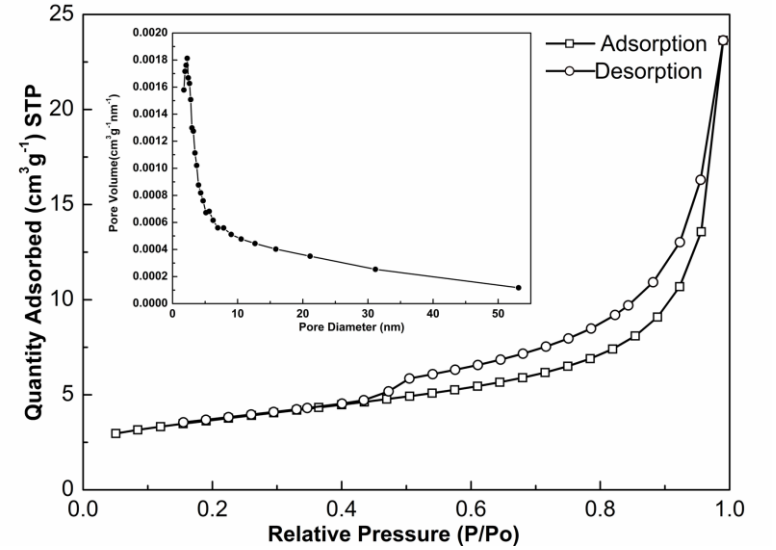

Figure 2. Nitrogen adsorption-desorption isotherms of the $LiFePO_4$ particles with the inset of pore size distribution.

Nitrogen adsorption-desorption isotherm of the $LiFePO_4$ sample is presented in Fig. 2, which corresponds to a type IV isotherm with an H3 hysteresis loop [6], and the inset is the pore size distribution calculated by Barret–Joyner–Halenda (BJH) model. The SSA of the $LiFePO_4$ sample is 12.55 m^2/g, and the average pore diameter is 13 nm. Moreover, it can be seen from the diagram that the pore size ranges largely from 2 to 4 nm, indicating the mesoporosity of $LiFePO_4$ particles according to IUPAC.

SEM images of the three different electrodes, LFP-CB, LFP-CNTs, LFP-GNs are presented in Fig. 3. As known, conductive additives provide conductive path from the current collector to the active material through the electrode [17]. It was illustrated that CB particles aggregate randomly on the surface of $LiFePO_4$ particles as shown in Fig. 3 (a) and (b), whose resistance is mainly dependent on the particle-to-particle contact. It can be ascribed to the point-to-point model, which means that the electric contact between $LiFePO_4$ particles and CB tends to weaken on account of the volume variation during the charge-discharge process. CNTs agglomerate to make fluffy conductive cluster surrounding

the $LiFePO_4$ particles with line-point contact as shown in Fig. 3 (c) and (d), making CNTs span irregularly in the electrode.

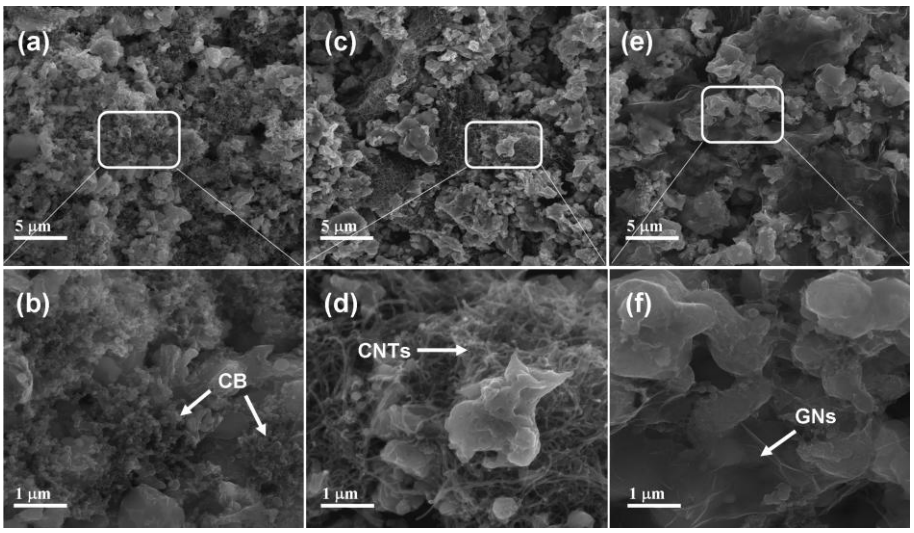

Figure 3. SEM images of the electrodes in plane: (a), (b) LFP-CB; (c), (d) LFP-CNTs; (e), (f) LFP-GNs.

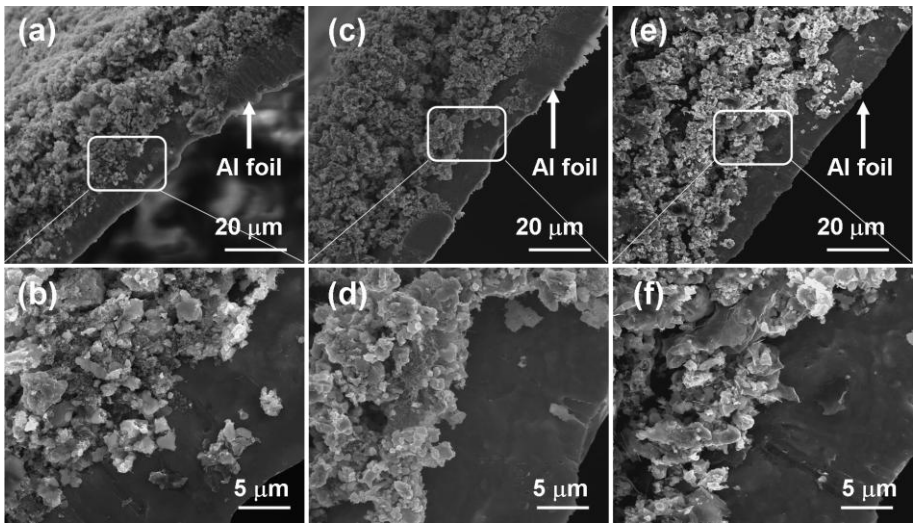

Figure 4. SEM images of the cross-section of electrodes: (a), (b) LFP-CB; (c), (d) LFP-CNTs; (e), (f) LFP-GNs.

GNs surround the $LiFePO_4$ particles by the virtue of their wrinkled and overlapped edges as well as flexible and planar structure to construct plane-to-point networks [18] as in Fig. 3 (e) and (f), leading to remarkable enhancement in the electrical conductivity. The large size and peculiar two-dimensional structure efficiently promote the probability of contact between active materials and conductive additives. The cross-section of the electrodes was illustrated in Fig. 4. CB particles have relatively better dispersion in $LiFePO_4$ particles than CNTs while GNs intimately contact with

$LiFePO_4$ particles, which are in accordance with Fig. 3. It can be demonstrated that GNs provide superior electron conveying channels and thus exhibit higher conductive efficiency.

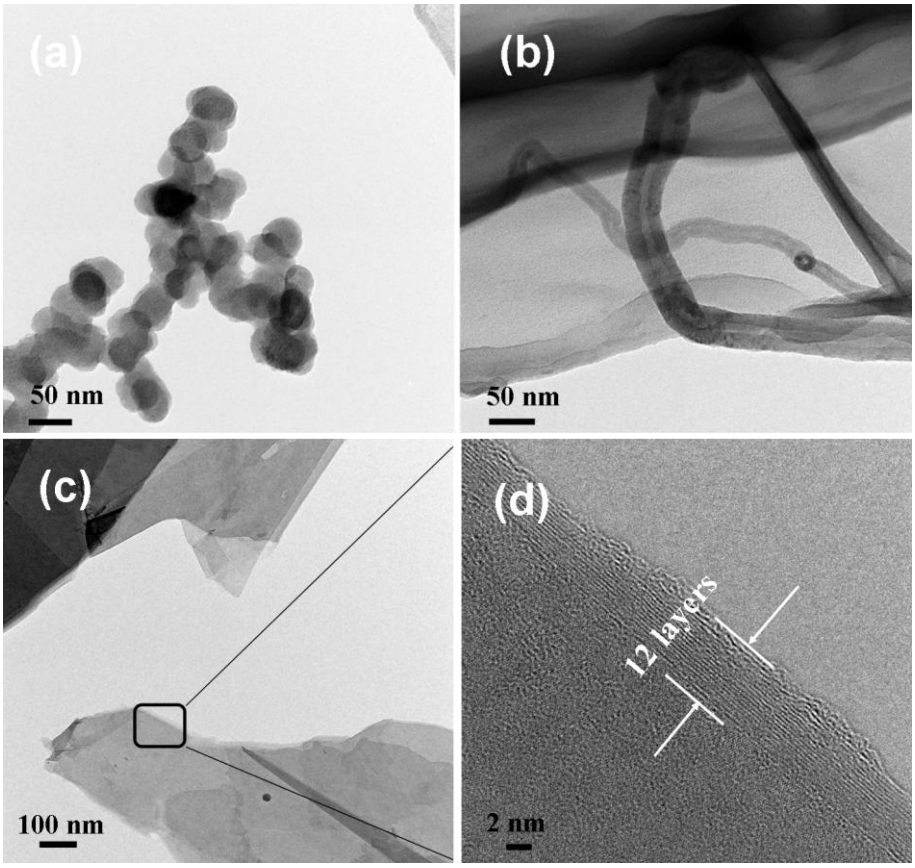

Figure 5. HRTEM images of carbon conductive additives: (a) CB; (b) CNTs; (c), (d) GNs.

HRTEM images are showed in Fig. 5 to further verify the microstructure of the carbonaceous conductive additives. Disordered CB chains are formed with dotted contact, resulting in low-efficient connection with active materials, especially under low addition. A few long individual bending CNTs can be seen in Fig. 5 (b), with an average outer diameter about 20 nm, and inner diameter about 5 nm. Both the electronic and the ionic conductivity of the electrode would be enhanced as the CNTs wires can percolate into the voids between the $LiFePO_4$ particles [17]. The marginal morphology of GNs, which are composed of 12 graphene layers, are exhibited in Fig. 5 (c) and (d). The large size of the platelets and wounded edges wrap $LiFePO_4$ particles and make firm coverage, providing the desirable electron transportation.

Electrochemical impedance measurement was carried out to investigate the electrochemical property of the three kinds of nanocomposites. The corresponding Nyquist profiles of the spectra are presented in Fig. 6 and the simple equivalent circuit was inset to simulate the situation. An intercept at the $Z`$ axis in high frequency corresponded to the solution resistance (*Rs*), which implies the electrolyte solution resistance and electric contact resistance, while the semicircle in the high and middle frequency range represented the charge transfer resistance (*Rct*). The sloping line in the low frequency

referred to the Warburg impedance (*Zw*), which is associated with lithium-ion diffusion in the $LiFePO_4$ bulk [7, 19]. Double layer capacitance and passive film capacitance are denoted as *Cd*. Apparently, LFP-GNs electrode shows the lowest charge transfer resistance, indicating the highest charge transfer rate, which can be assigned to the intimately electric contact (as shown in Fig. 3 (e), (f)). Both LFP-CNTs and LFP-GNs electrode show larger slope than LFP-CB electrode, implying the enhancement of the electrochemical activity of $LiFePO_4$, which is attributed to the better conductive networks [18].

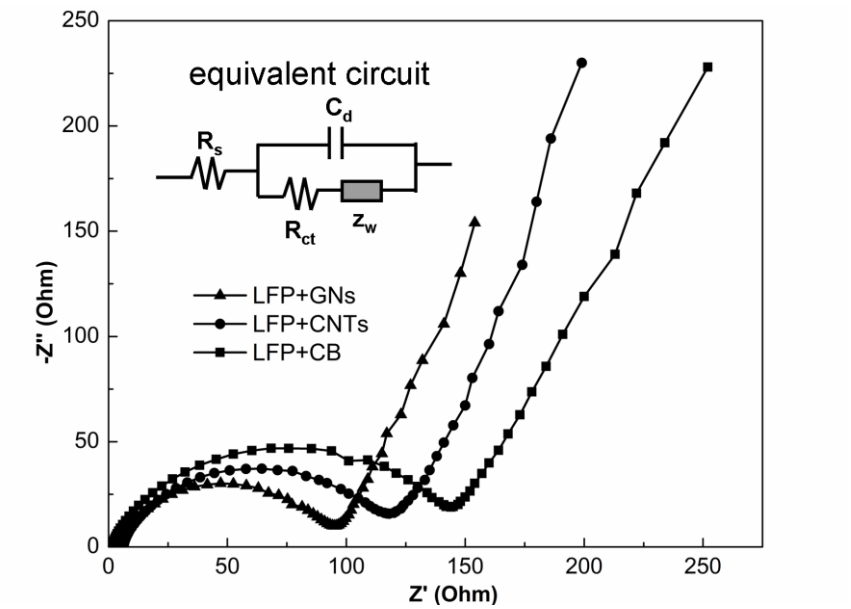

Figure 6. EIS Nyquist plots of LFP-CB, LFP-CNTs and LFP-GNs in the frequency ranges from 100 kHz to 0.1 Hz.

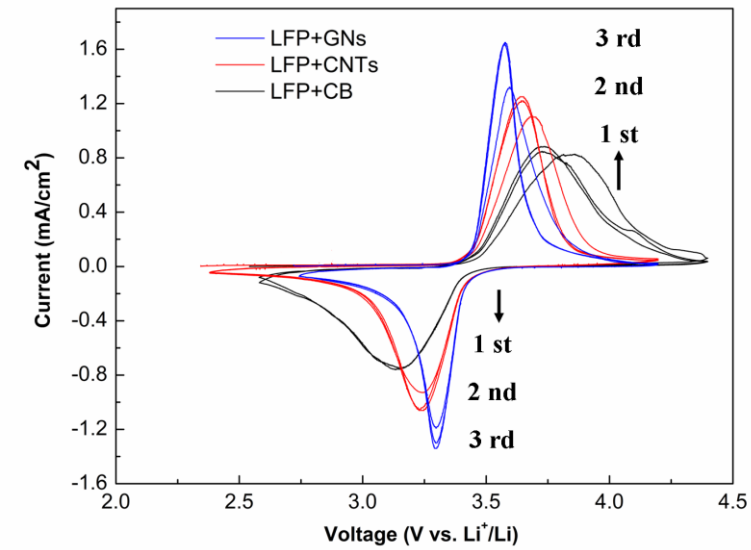

Figure 7. Cyclic voltammograms of the first 3 cycles of (a) LFP-CB, (b) LFP-CNTs, (c) LFP-GNs in 1 M $LiPF_6$ / EMC-DEC (1:1 in v/v) at the scanning rate of 0.05 mV/s.

Cyclic voltammograms curves are presented in Fig. 7. There is only one oxidation peak and one reduction peak for each cycle, proving only one redox reaction during the insertion and extraction of lithium ions. The anodic and cathodic peaks corresponds to the charge–discharge reaction of the Fe^{2+}/Fe^{3+} redox couple accompanied with phase transformation [2]. The peak separation exhibited by the LFP-GNs was 0.35 V, much smaller than that of LFP-CNTs and LFP-CB, owing to its lower polarization. The anodic and cathodic peaks appear approximately symmetrical. As the cycle number increased, the anodic and cathodic peak exhibit gradually increasing intensity and narrower peak due to the activation of $LiFePO_4$ cathode. This is in accordance with the former ones (except the first cycle), suggesting good insertion/extraction reversibility of the electrodes, especially in the LFP-GNs electrode [20].

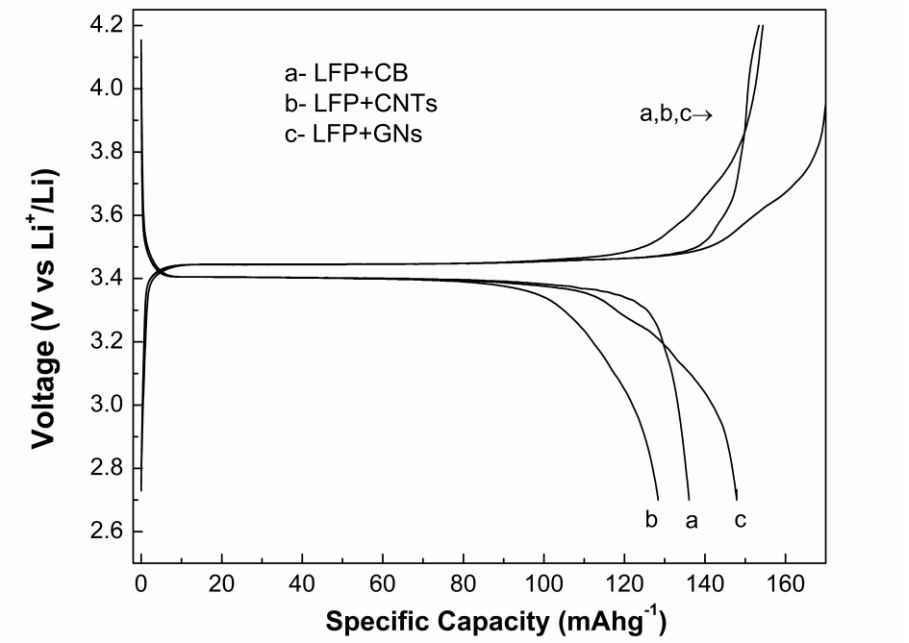

Figure 8. The first charge-discharge profile at 0.1 C of LFP-CB, LFP-CNTs, LFP-GNs.

The initial charge and discharge profiles at 0.1 C of LFP-CB, LFP-CNTs, LFP-GNs are exhibited in Fig. 8. It can be clearly observed that all the three electrodes had irreversible capacity loss in the first cycle. However, LFP-GNs electrode had the highest charge-discharge capacity, which can be ascribed to the better electrochemical reaction activity. More interestingly, LFP-CNTs electrode exhibited shorter flat plateau, presumably resulted from the poor dispersion of CNTs as well as slight hydroxylation, they likely tangle with each other and gather to form bundles and clusters (shown in Fig. 3 (c), (d)) thus block the electrochemical reaction activation of $LiFePO_4$ to some extent.

The cycle performance of LFP-CB, LFP-CNTs, LFP-GNs is showed in Fig. 9, as can be seen, LFP-GNs showed the most outstanding performance among them (146 mAh g^{-1} at 0.1 C and 125 mAh g^{-1} at 1 C), which can be attributed to the improved electrical conductivity by GNs addition. The specific capacity of LFP-CB is 135 mAh g^{-1} at 0.1 C and 115 mAh g^{-1} at 1 C. But that of LFP-CNTs is

much lower, 127 mAh g^{-1} at 0.1 C and 102 mAh g^{-1} at 1 C, which is presumably ascribed to the lower electrochemical reactions activity due to the inhomogeneous distribution of CNTs in $LiFePO_4$.

4. CONCLUSIONS

Carbon black, CNTs and graphene nanosheets were added into olivine-type $LiFePO_4$ particles as conductive additives. Owing to the superior plane-to-point networks, GNs can provide sufficient electric contact with active materials, thus significantly enhance the electrochemical performance of $LiFePO_4$ material. Compared with LFP-CB, LFP-CNTs showed high conductivity which could be ascribed to the better line-to-point contact than point-to-point contact, but the relatively low specific capacity was probably due to the inhomogeneous distribution. The practice application of GNs in lithium-ion batteries would be highly developed if GNs could be large-scale produced.

ACKNOWLEDGEMENTS
This work is financially supported by the Fundamental Research Funds for the Central Universities of China (No.CDJZR10 13 88 01 & No.CDJXS10 13 11 58) and National Natural Science Foundation of China (No.51172293), and technically supported by the Center of New-Energy Materials, Chongqing University, China.

References

1. V. Etacheri, R. Marom, R. Elazari, G. Salitra and D. Aurbach, *Energy Environ. Sci.*, 4 (2011) 3243.
2. A.K. Padhi, K.S. Nanjundaswamy and J.B. Goodenough, *J. Electrochem. Soc.*, 144 (1997) 1188.
3. K. Saravanan, M.V. Reddy, P. Balaya, H. Gong, B.V.R. Chowdari and J.J. Vittal, *J. Mater. Chem.*, 19 (2009) 605.
4. X.L. Wu, L.Y. Jiang, F.F. Cao, Y.G. Guo and L.J. Wan, *Adv. Mater.*, 21 (2009) 2710.
5. J. Liu, T.E. Conry, X.Y. Song, M.M. Doeff and T.J. Richardson, *Energy Environ. Sci.*, 4 (2011) 885.
6. Y. Ren and P.G. Bruce, *Electrochem. Commun.*, 17 (2012) 60.
7. C. Su, X.D. Bu, L.H. Xu, J.L. Liu and C. Zhang, *Electrochim. Acta*, 64 (2012) 190.
8. J.J. Wang and X.L. Sun, *Energy Environ. Sci.*, 5 (2012) 5163.
9. M.M. Doeff, Y.Q. Hu, F. McLarnon and R. Kostecki, *Electrochem. Solid-State Lett.*, 6 (2003) A207.
10. X.L. Li, F.Y. Kang, X.D. Bai and W.C. Shen, *Electrochem. Commun.*, 6 (2007) 663.
11. J.Q. Zhao, J.P. He, J.H. Zhou, Y.X. Guo, T. Wang, S.C. Wu, X.C. Ding, R.M. Huang and H.R. Xue, *J. Phys. Chem. C*, 115 (2011) 2888.
12. M. Yang and Q.M. Gao, *J. Alloys Compd.*, 509 (2011) 3690.
13. S.Y. Chung, J.T. Bloking and Y.M. Chiang, *Nat. Mater.*, 1 (2002) 123.
14. J. Lim, J. Gim, S.W. Kang, S. Baek, H. Jeong and J. Kim, *J. Electrochem. Soc.*, 159 (2012) A479.
15. J.H. Park, S.Y. Lee, J.H. Kim, S. Ahn, J.S. Park and Y.U. Jeong, *J. Solid State Electrochem.*, 14 (2009) 593.
16. W.S. Hummers and R.E. Offeman, J. Am. Chem. Soc., 80 (1958) 1339.
17. U. Dettlaff-Weglikowska, J. Yoshida, N. Sato and S. Roth, *J. Electrochem. Soc.*, 158 (2011) 174.

18. F.Y. Su, C.H. You, Y.B. He, W. Lv, W. Cui, F.M. Jin, B.H. Li, Q.H. Yang and F.Y. Kang, *J. Mater. Chem.*, 20 (2010) 9644.
19. Y.F. Tang, F.Q. Huang, H. Bi, Z.Q. Liu and D.Y. Wan, *J. Power Sources*, 203 (2012) 130.
20. G.X. Wang, H. Liu, J. Liu, S.Z. Qiao, G.M. Lu, P. Munroe and H. Ahn,. *Adv. Mater.*, 22 (2010) 4944.